

## Surface Effects on the Energy Gap in Nuclear Matter

*K. Amos and F. Robbins*

School of Physics, University of Melbourne, Parkville, Vic. 3052.

### *Abstract*

The energy gap in the intrinsic excitation spectra of even-even nuclei is calculated in the BCS approximation starting from separable interactions adjusted to fit  $^1S_0$  nucleon scattering data. Simplified nuclear models are used to investigate the relation between the surface properties and the value of the energy gap in finite nuclei and, in particular, we consider a slab model of infinite extent in two directions but finite in the third direction and of variable surface thickness. An effective length of the slab is defined and this is held constant while the density profile is varied. For a fixed effective mass, it is found that the energy gap is essentially determined by the effective length for a particular interaction. On the other hand, radically diverse variations of the energy gap with effective length are obtained for potentials that differ appreciably in their repulsive character in infinite nuclear matter. This sensitivity may be fortuitous however, as the slab model underestimates the finite volume contribution to the pairing matrix elements and overestimates the importance of the infinite matter properties of the potential.

### 1. Introduction

It has long been known that the energy gap in infinite nuclear matter exists but is small, at the very most a few tenths of an MeV, and is even less if a reduced value of the effective mass is considered. Specifically, solutions of the energy gap equation (Emery and Sessler 1960; Ishihara *et al.* 1963) have shown that, for a variety of interactions including the hard-core Gammel-Thaler interaction and classes of separable interactions, the energy gap exists in infinite matter for larger values of the effective mass provided that the Fermi momentum lies between  $0.2$  and  $1.4 \text{ fm}^{-1}$ . In those studies it was not possible to place limits on the magnitude of the energy gap since that magnitude is a sensitive function of parameters involved in the calculations than were not sufficiently well known.

Nevertheless, it was evident that the energy gap in infinite nuclear matter was very much less than that observed in any heavy even-even nucleus.

The earliest attempt (Thompson 1965; Thompson and Waghmare 1966) to explain this discrepancy used simplified, infinite potential well models of the nuclear field. Furthermore, simplified inter-nucleon interactions (attractive delta functions) were used and were restricted to act only within a thin (momentum) shell about the Fermi surface. Nevertheless, by adjusting the strength of the delta functions in different regions of the Periodic Table, both the magnitude and shell structure oscillations of the pairing energy data (Nemirovsky and Adamchuk 1962) could be fitted. But these calculations failed to indicate whether the more realistic (albeit phenomenological) finite range interactions then employed in nuclear matter calculations of the energy

gap could also reproduce this pairing energy data. Subsequently, calculations (Kennedy *et al.* 1964a, 1964b; Kennedy 1966a, 1966b) using separable interactions chosen to fit S-wave nucleon–nucleon scattering data were made using a ‘slab’ model of the nucleus, in which the nuclear field is infinite in two directions but finite in the third. In these calculations, sums in the BCS integral equation for the energy gap were approximated by integrations with the consequence that shell structure effects on the energy gap could not be reproduced. However, by equating the semi-infinite slab to the liquid drop model (LDM) of a nucleus of the same surface area to volume ratio, a smooth variation of the energy gap with the atomic mass number of the LDM nucleus could be obtained fitting the mean variation of the empirical pairing energies in nuclei.

It has been suggested (Jakeman and Moszkowski 1966; Stepien and Szymanski 1968) that the nuclear surface region might be important in contributing to the enhanced energy gap in finite nuclei. This conjecture received support from the calculations (Emery and Sessler 1960; Ishihara *et al.* 1963) on low density nuclear matter which showed that for values of the Fermi momentum about  $0.8 \text{ fm}^{-1}$  the energy gap was of the order of several MeV. Further support for this idea was given by calculations (Kennedy *et al.* 1964a, 1964b; Kennedy 1966a, 1966b) on a high density edge slab model in that an energy gap resulted which was very much less than that of the corresponding low density edge slab. Also, at one time, experimental evidence (Griffin 1963; Britt *et al.* 1965; Moretto *et al.* 1969) on certain fissioning even–even nuclei appeared to indicate the presence of an enlarged energy gap at the fission saddle point where nuclear surface areas are large. Later experiments (Kuvatov *et al.* 1970; Natowity and Chulick 1971) lowered the estimate of this enhancement in some cases but the possibility of an energy gap strongly dependent on surface area still could not be refuted.

To investigate surface variation effects on the energy gap value, it is inappropriate to use the original slab model approach (Kennedy *et al.* 1964a, 1964b; Kennedy 1966a, 1966b) as the infinite well always yields too rapid a density variation at the surface. However, the simple model can be modified to permit a study of ‘realistic’ surface effects on the energy gap by using a finite value slab model potential associated with which is a surface density profile more diffuse than that of the infinite well model. But even for a finite potential model, the continuum states (in the BCS approximation) cannot contribute to the energy gap (Henley and Wilets 1963) and to regain their effect it is necessary either to replace the bare nucleon–nucleon interaction by a  $t$  matrix or, more generally, to resort to a higher order pairing theory. Because such extensions of finite nucleus calculations are very complicated, we have considered instead a model consisting of an infinite potential well of variable slope thereby permitting an arbitrarily diffuse surface region. The model which we have chosen is described in detail in the next section and the solutions its use yields to the energy gap equation are discussed thereafter.

## 2. Finite Well Slab Model

We consider a ‘slab’ of nuclear matter created by filling, to a Fermi sea, single particle states as defined by a single particle potential

$$\begin{aligned} V \rightarrow \infty & \text{ if } |x|, |y| > \frac{1}{2}S^{\frac{1}{2}} \\ & = (\hbar^2 k_F^2 / 2mZ_0)[z \Theta(z) - (z+L)\{1 - \Theta(z-L)\}], \end{aligned} \quad (1)$$

in which  $S^{\frac{1}{2}}$  is the width of the slab in the  $x$  and  $y$  directions, and  $L$  is the corresponding length of the slab in the  $z$  direction in the limit that the diffuseness parameter  $Z_0$  vanishes. The value of the Fermi momentum  $k_F$  we choose to be  $1.4 \text{ fm}^{-1}$ , and in the limit of  $S \rightarrow \infty$ , the wavefunctions of the model are given by

$$\psi = S^{-\frac{1}{2}} A(k_z) \phi(k_z, z) \exp(i k_x x + i k_y y), \quad (2)$$

where  $A(k_z)$  is determined from the normalization of the wavefunction. The functions of  $z$  are solutions of

$$\partial^2 \phi / \partial^2 z + (k_z^2 - 2mV/\hbar^2) \phi = 0. \quad (3)$$

Continuity of these ( $z$  dependent) wavefunctions at the  $z = 0$  and  $-L$  boundaries determines that

$$\begin{aligned} \phi = & \{1 - \Theta(z)\} \Theta(z-L) \sin(k_z z + \delta) \\ & + \{\sin \delta / \text{Ai}(-K)\} [\Theta(z) \text{Ai}(gz - K) + \{1 - \Theta(z-L)\} (-)^l \text{Ai}\{g(-z-L) - K\}], \end{aligned} \quad (4)$$

where

$$K = (Z_0/k_F^2)^{2/3} k_z^2, \quad g = (k_F^2/Z_0)^{1/3}, \quad (5)$$

$$\tan \delta = (Z_0/k_F^2) k_z \text{Ai}(-K) / \text{Ai}'(-K) \quad (6)$$

with Airy functions  $\text{Ai}(t)$ , and states of even and odd parity are classified by the  $l$  values 0 and 1 respectively. The symmetry about  $z = -\frac{1}{2}L$  provides the condition

$$k_z = (n_z \pi + 2\delta)L, \quad (7)$$

and normalization of the single particle wavefunctions is achieved when

$$A(k_z) = (\frac{1}{2}L + 2Z_0 k_z^2/k_F^2 - \sin 2\delta/2k_z)^{-\frac{1}{2}}. \quad (8)$$

In the thermal or non-superfluid state approximation, the nuclear density is defined by

$$\rho(\mathbf{r}) = 4 \sum_{k < k_F} \psi^* \psi, \quad (9)$$

in which equal numbers of protons and neutrons have been assumed. In the limit of large  $L$

$$\rho(\mathbf{r}) \rightarrow \frac{4S}{2\pi^3} \int d\mathbf{k} |\psi|^2, \quad (10)$$

from which one obtains

$$\rho(z) = \frac{1}{2\pi^2} \int_0^{k_F} dk_z (k_F^2 - k_z^2) |\phi(k_z, z)|^2. \quad (11)$$

Thus in the inner region of the (large) slab the density approaches a constant value of

$$\rho(\infty) = \frac{1}{4\pi^2} \int_0^{k_F} dk_z (k_F^2 - k_z^2) = \frac{k_F^3}{6\pi^2}. \quad (12)$$

It is convenient to define an effective length  $L^*$  of the slab in the  $z$  direction by writing (Kennedy *et al.* 1964a, 1964b; Kennedy 1966a, 1966b)

$$L^* = L + 2\delta L, \quad (13)$$

where the correction to the length  $2\delta L$  is obtained by requiring a large box of nuclear matter of length  $2X + 2\delta L$  and constant density  $\rho(\infty)$  to contain the same number of nucleons as a slab with  $L = 2X$ , the same cross sectional area and density given by  $\rho(z)$ . In the limit that  $X$  approaches infinity, the relation

$$\rho(\infty)(X + \delta L) = \int_{-X}^{\infty} dz \rho(z) \quad (14)$$

results, and by substituting for  $\rho(z)$  and upon interchanging the order of integration, one obtains

$$\delta L = -\frac{3\pi}{8k_F} + \frac{2Z_0}{5} - \frac{3}{2k_F^3} \int_0^{k_F} dk_z \frac{(k_F^2 - k_z^2) \sin 2\delta}{2k_z}. \quad (15)$$

In the large  $Z_0$  limit ( $> 2.5$ ) the asymptotic expansions for the Airy functions for large negative argument can be used to ascertain that

$$\delta \approx -\left\{ \frac{1}{4}\pi + \frac{2}{3}Z_0(k_z/k_F)^3 \right\}, \quad (16)$$

and then

$$\delta L \approx \frac{2}{5}Z_0. \quad (17)$$

Density profiles  $\rho(z)/\rho(\infty)$  for various values of  $Z_0$  with  $L^*$  kept at the values of 4 and 8 fm are shown in Figs 1a and 1b respectively, from which it should be noted that a skin thickness of 2.4 fm, as is appropriate for heavy nuclei, and a realistic form factor shape occur when  $Z_0$  has the value of 3.25 fm, with  $L^*$  being 8 fm. As  $Z_0$  increases, the particle density spreads to larger radii with the increase in the skin thickness being almost linear. But the chosen value of  $L^*$  is much larger than a connection between a slab model and real nuclei (Kennedy *et al.* 1964a, 1964b; Kennedy 1966a, 1966b), namely

$$L^* = \frac{2}{3}r_0 A^{1/3}, \quad (18)$$

which was obtained by equating the surface area to volume ratio of a semi-infinite slab of nuclear matter of length  $L^*$  to that of the corresponding LDM nucleus. For  $^{208}\text{Pb}$  and using the standard radius  $r_0$  of 1.1 fm, this yields a value of 4.4 fm for  $L^*$  and the profiles in Fig. 1 for this case are not like the measured (electron scattering) form factors for this nucleus. However, the skin thickness and profiles as shown in Fig. 1b for  $L^* = 8$  fm are appropriate in scale for the heavy nuclei and thus our model may serve as a test of density dependent effects upon the energy gap.

In the BCS approximation, the energy gap is a solution of the integral equation

$$\Delta(k) = -\frac{1}{2} \sum_{k'\sigma'} G(k, \sigma, t, k', \sigma', t') \{ \hat{\epsilon}^2(k') + \Delta^2(k') \}^{-\frac{1}{2}} \Delta(k'), \quad (19)$$

where  $G$  is the properly antisymmetrized pairing matrix element for scattering in time reversed orbitals of protons (neutrons) that are interacting through a potential, namely

$$G(k, \sigma, t, k', \sigma', t') = \delta_{tt'} \langle k\sigma, -k-\sigma | V | k'\sigma', -k'-\sigma' \rangle - \langle -k'-\sigma', k'\sigma' \rangle. \quad (20)$$

In equation (19),  $\hat{\epsilon}(\mathbf{k})$  is the single particle energy in the absence of pairing and measured from the Fermi surface. This has not been calculated within the framework of the slab model but instead is defined in the effective mass approximation by

$$\hat{\epsilon}(\mathbf{k}) = \hbar^2(k^2 - k_F^2)/2m^* \quad (21)$$

and, in lieu of a reliable estimate, the effective mass  $m^*$  has been treated as arbitrarily adjustable to fit the pairing energies in nuclei.

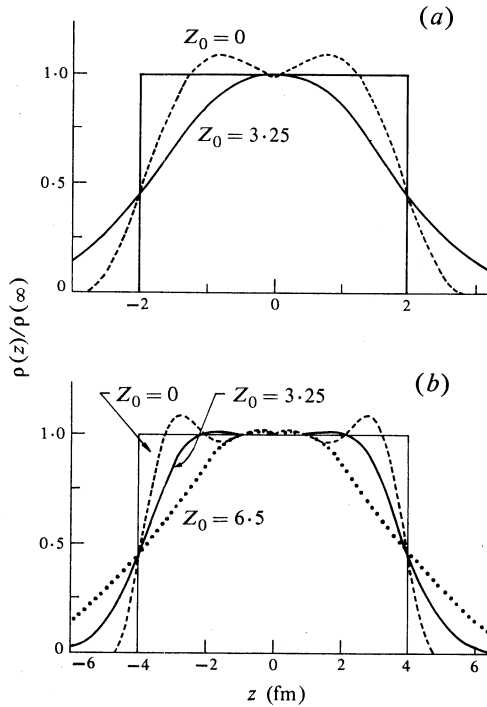


Fig. 1. Density profiles as a function of  $z$  for the effective length (a)  $L^* = 4$  and (b)  $L^* = 8$ , and for various values of the diffuseness parameter  $Z_0$ .

As the short range part of the nucleon–nucleon interaction is most essential to the pairing effect, the potential  $V$  is represented by an S-wave interaction; the most important contribution to  $V$  at short distances. Two different phenomenological forms of this interaction have been used in our calculations, the first of these being the ‘back to back Yamaguchi’ interactions that have been used previously by Kennedy and which have the form

$$V(r, r') = \frac{\pi \hbar^2}{2m} \left( \frac{\lambda_1 \exp(-\beta_1 r) \exp(-\beta_1 r')}{r r'} - \frac{\lambda_2 \exp(-\beta_2 r) \exp(-\beta_2 r')}{r r'} \right), \quad (22)$$

with parameters  $\lambda_i, \beta_i$  chosen to fit the S-wave pp scattering data; to wit the effective range, scattering length and phase shift at 310 MeV. With three numbers to fit and four adjustable parameters, an infinite family of such potentials can be defined by

arbitrarily choosing the parameter  $\beta_1$ . In Table 1 three such potentials are given (labelled Y1, Y2 and Y3) which correspond to very different values of the parameter  $\lambda_1$ . As well as the Yamaguchi interactions we have considered a separable gaussian interaction (Strobel 1968), denoted as potential G, and which was chosen to fit the pp effective range, scattering length and  $^1S_0$  phase shifts up to a lab energy of 300 MeV. The form of this potential is

$$V(r, r') = (\hbar^2/m) \{ \lambda_1 \exp(-\alpha_1 r^2) \exp(-\alpha_1 r'^2) - \lambda_2 \exp(-\alpha_2 r^2) \exp(-\alpha_2 r'^2) \}, \quad (23)$$

and the appropriate values of the parameters are given in Table 1 also.

**Table 1. Parameter values of Yamaguchi (Y) and Gaussian (G) types of interactions**

Type	$\lambda_1$	$\beta_1(\alpha_1^{\frac{1}{2}})$	$\lambda_2$	$\beta_2(\alpha_2^{\frac{1}{2}})$
Y1	7.655	3.0	1.731	1.766
Y1T	54.85	4.5	4.458	2.119
Y2	25.83	4.5	1.023	1.645
Y3	123.1	6.0	0.953	1.62
G	12260	4.56	2.987	0.844

If the sum over the spin states in the gap equation is completed, one is left with the direct part of the pairing matrix element, namely

$$G(\mathbf{k}, \mathbf{k}') = \langle \mathbf{k}, -\mathbf{k} | V | \mathbf{k}', -\mathbf{k}' \rangle, \quad (24)$$

and, for the slab model geometry, these matrix elements can be expressed in terms of the most natural variables  $k_z$  and  $k_{\perp} = (k_x^2 + k_y^2)^{\frac{1}{2}}$  for both the Yamaguchi and gaussian forms of the interaction, and which are amenable for evaluation. Details of the derivations are given in the Appendix. While these variables are convenient for evaluation of the matrix elements, solution of the gap equation is most conveniently achieved by using spherical polar coordinates, the standard conversion of discrete summations over momenta into integrations and the Kennedy partial linearization technique in which the denominator of the integrand is replaced by  $|\hat{\epsilon}(\mathbf{k}')|$  in all but a thin shell of width  $2k_c$  (chosen as  $0.2 \text{ fm}^{-1}$ ) about the Fermi momentum. Within the shell all quantities are set to their Fermi momentum values except  $\hat{\epsilon}$  which is chosen to be

$$\hat{\epsilon}(\mathbf{k}) = \hbar^2 k_F (k - k_F) / m^*, \quad (25)$$

whence

$$\begin{aligned} \Delta(\mathbf{k}) = & \frac{-S}{2\pi^2} \int_0^1 d(\cos \theta') \left\{ \frac{2m^* k_F}{\hbar^2} \Delta(\mathbf{k}'_F) A^{-2}(\mathbf{k}'_F) G(\mathbf{k}_F, \mathbf{k}'_F) \ln \left( \frac{2\hbar^2 k_F k_c}{m^*} \Delta(\mathbf{k}_F) \right) \right. \\ & \left. + \left( \int_0^{k_F - k_c} + \int_{k_F + k_c}^{\infty} \right) dk' k'^2 A^{-2}(\mathbf{k}') G(\mathbf{k}, \mathbf{k}') \Delta(\mathbf{k}') |\hat{\epsilon}(\mathbf{k}')|^{-1} \right\}, \quad (26) \end{aligned}$$

which is conveniently solved by using gaussian quadrature schemes to recast the gap equation into the matrix

$$\Delta = \mathbf{A} \cdot \mathbf{F},$$

in which  $\mathbf{A}$  is the appropriate  $n$  by  $n$  square matrix ( $n = 113$  was chosen), acting upon the column matrix  $\mathbf{F}$  defined by

$$F_i = \Delta_i \ln(2\hbar^2 k_F k_c / m^* \Delta_i) \quad i = 1, \dots, m, \quad (27a)$$

$$= \Delta_i \quad i = m+1, \dots, n. \quad (27b)$$

In most evaluations the value 10 was chosen for  $m$  although tests were made using values of 4 or 6 to ensure that the precise choice was of little consequence. Then with

$$\mathbf{B} = (\mathbf{1} - \mathbf{A})^{-1} \mathbf{A}, \quad (28)$$

we have

$$\Delta = \mathbf{B} \cdot (\mathbf{F} - \Delta), \quad (29)$$

which is a set of  $m$  nonlinear equations that we will solve using the Newton-Raphsen method.

### 3. Density Independent Effective Mass Results

The gap equation has been solved for each of the S-wave separable potentials described previously and the gap  $2\Delta(k_F \cos \theta)$  found as a function of the effective length  $L^*$  and effective mass  $m^*$  for a sequence of density distributions extending from the sharply surfaced slab model ( $Z_0 = 0$ ) through to a very diffuse edge slab model ( $Z_0 = 7$ ). For each potential, results have been obtained in two different ways; the first with  $L^*$  as the independent variable and  $Z_0$  being fixed; the second with  $Z_0$  as the independent variable and fixed  $L^*$ .

When  $Z_0$  was fixed (values of 0 and 3.25 were used) the variation of the gap equation with  $k_z$  for several values of  $L^*$  and  $m^*$  for the Y1 and G interactions are very similar, whence only the G interaction results are shown in Fig. 2. From this

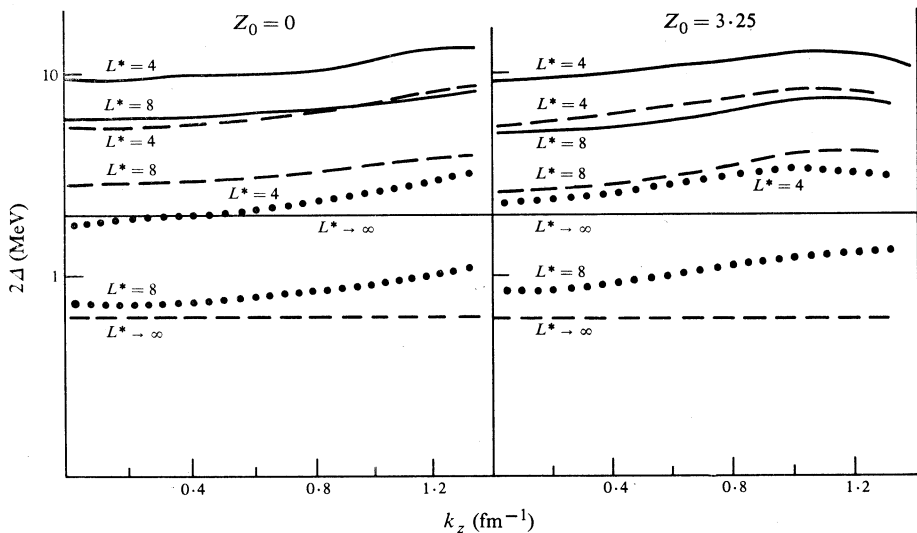


Fig. 2. Energy gap  $2\Delta$  as a function of  $k_z$  ( $k_F \cos \theta$ ) for the gaussian interaction G for two values of the parameter  $Z_0$ , for three values of the effective length and for three values of the effective mass:  $m^*/m = 1$  (solid curve); 0.8 (dashed curve); 0.6 (dotted curve).

figure it is clear that the energy gap increases as slab thickness is reduced for particular values of  $Z_0$  and  $m^*$ , and hence, at least qualitatively, the nature of these solutions is similar to that of the simple slab model. The main features of these solutions then are the enhancement of the energy gap over the infinite matter value for finite  $L^*$ , the extreme sensitivity of the energy gap to the parameters  $m^*$  and  $L^*$  when the gap is small and the reduction of this sensitivity when the gap is large. It is to be noted that for both values of  $Z_0$  used, the solutions of the gap show only minor variations for fixed  $m^*$  and  $L^*$ .

Now, while in the case of the potential Y1 and  $Z_0 = 0$  our results agree entirely with those of Kennedy *et al.* (1964a, 1964b) and Kennedy (1966a, 1966b), there is a striking disagreement between our calculations for the potential Y3. Our solutions displayed in Fig. 3 show for the simple slab model a *decrease* of the energy gap below the infinite matter limit. Indeed as  $m^*$  is reduced the numerical solutions become negative at smaller values of  $\cos\theta$  and hence these can no longer be considered as meaningful solutions for the energy gap which must be taken to vanish for all angles.

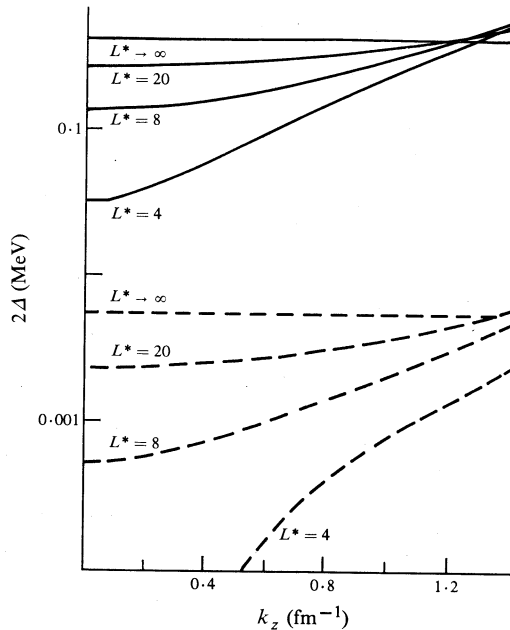


Fig. 3. Energy gap  $2\Delta$  as a function of  $k_z$  ( $k = k_F$ ) for the Y3 interaction and for four values of the effective length. Here  $Z_0 = 0$  and two values of the effective mass are used:  $m^*/m = 1$  (solid curves);  $0.8$  (dashed curves).

The energy gap  $2\Delta$  which has been angle averaged (over  $\cos\theta$ ) for the interactions Y1 and Y3 is plotted as a function of  $L^*$  for selected values of  $m^*$  and  $Z_0$  in Fig. 4. The results for interactions G and Y2 are very similar to those for Y1. In Fig. 4b the portions of these curves marked with asterisks indicate extrapolations since for these regions of  $L^*$  and  $m^*$  acceptable solutions of the gap equation cannot be found other than the trivial zero value.

It is noted that although realistic solutions may cease to exist, the angle averaged curves show a continuous behaviour and in some cases actually increase. Hence

it is reasonable to suppose that the vanishing of the energy gap in such cases is connected with the behaviour of the pairing matrix elements at small values of  $\cos\theta$ . Support for this conjecture comes from consideration of the 'partially' angle averaged finite- $L$  contributions to the pairing matrix elements, namely

$$\bar{G}(k, k', \cos\theta) = \int_0^1 d(\cos\theta') \{A^{-2}(k \cos\theta) G_{L^*}(\mathbf{k}, \mathbf{k}') - (2/L) G_\infty(\mathbf{k}, \mathbf{k}')\}, \quad (30)$$

which are repulsive for the potential Y3 but essentially attractive for the potential Y1 at small values of  $\cos\theta$ . Both are attractive for large values of  $\cos\theta$ . This anisotropy occurs because at low values of  $\cos\theta$  the finite effective length contributions to the pairing matrix element have the same behaviour as the infinite matter pairing matrix element between the states  $k$  and  $k'$ , while at larger values of  $\cos\theta$  these corrections are influenced strongly by the changes in the  $k_z$  wavefunctions.

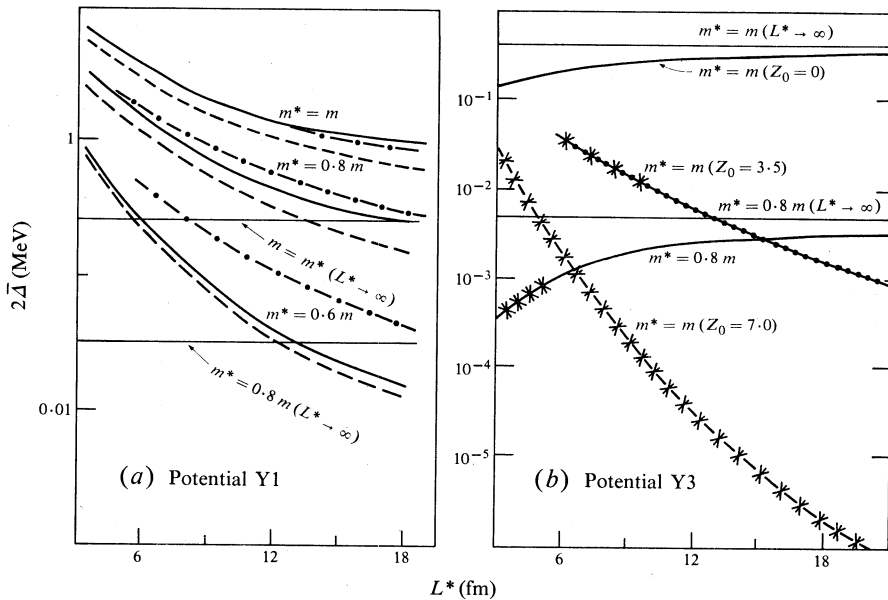


Fig. 4. Angle averaged energy gaps  $2\bar{\Delta}$  for the interactions (a) Y1 and (b) Y3 as functions of the effective length  $L^*$  for various values of the effective mass and parameter  $Z_0$ . In (a) the solid curves are for  $Z_0 = 0$ ; dashed curves,  $Z_0 = 3.25$ ; dot-dash curves,  $Z_0 = 7.0$ .

If we then average these results over  $\cos\theta$ , we get the Fourier components for potentials Y1 and Y3 displayed in Fig. 5. A clear correlation emerges between the repulsive character of these Fourier components and the behaviour of the angle averaged energy gap, namely that the larger the amount of attraction in these finite  $L^*$  contributions the greater the increase in the angle averaged gap. Our results differ markedly from those of Kennedy *et al.* (1964a, 1964b) and Kennedy (1966a, 1966b) in the extent to which this effect is observed. For example, in our calculations for the potential Y3, the angle averaged gap actually decreases as  $L^*$  is reduced and eventually vanishes; a result one expects for an interaction with strong repulsion and in the limit  $L \rightarrow 0$ . Kennedy's results are nebulous on this point.

The mean variation with mass of empirical pairing energies (Nemirovsky and Adamchuk 1962) for  $A > 40$  is given (in MeV) by

$$\langle \delta E \rangle = 16 \cdot 97 A^{-0.56395}, \quad (31)$$

and is chosen to be the energy gap value at the Fermi momentum. It is possible to fit this variation with the slab model by varying the effective mass for each interaction and using the LDM nuclear mass to effective length relationship specified previously. For potentials G and Y1, using a slope parameter ( $Z_0$ ) value of zero, a good fit to this mass variation requires effective masses of 0.535 and 0.804 respectively. With a slope parameter value of 3.25 fm, effective masses of 0.59 and 0.764 were required and a value of 0.863 was needed for a calculation made using the Y2 potential. These variations are shown in Fig. 6. No results are given for the potential Y3 as its use led to the wrong type of mass variation.

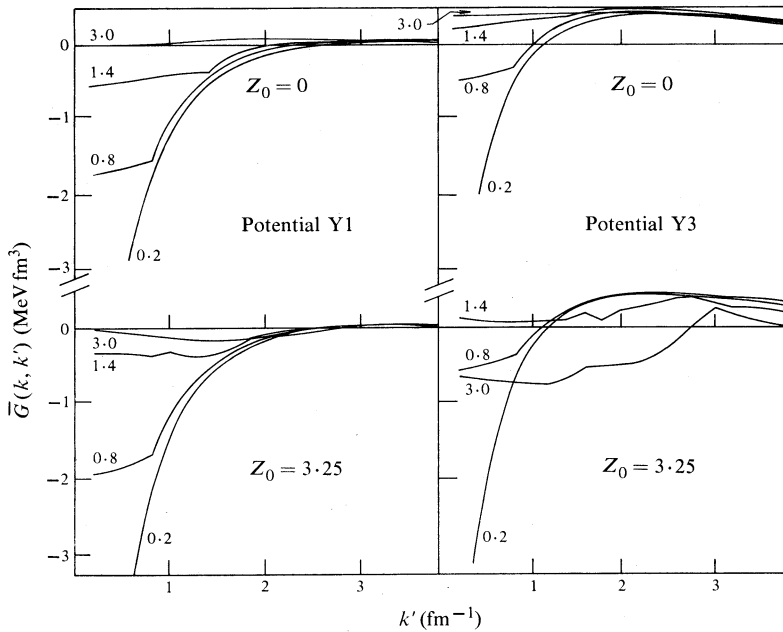
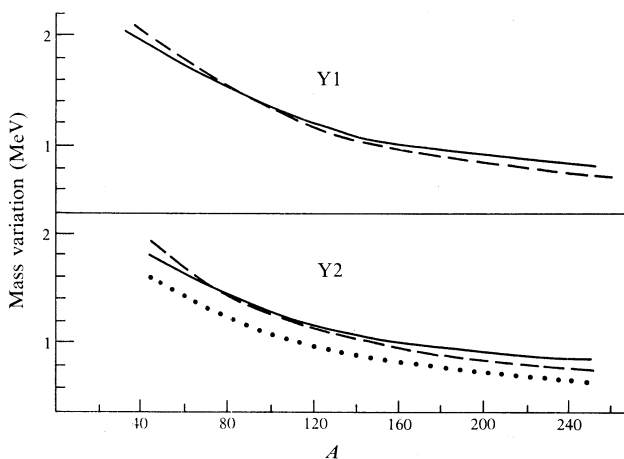
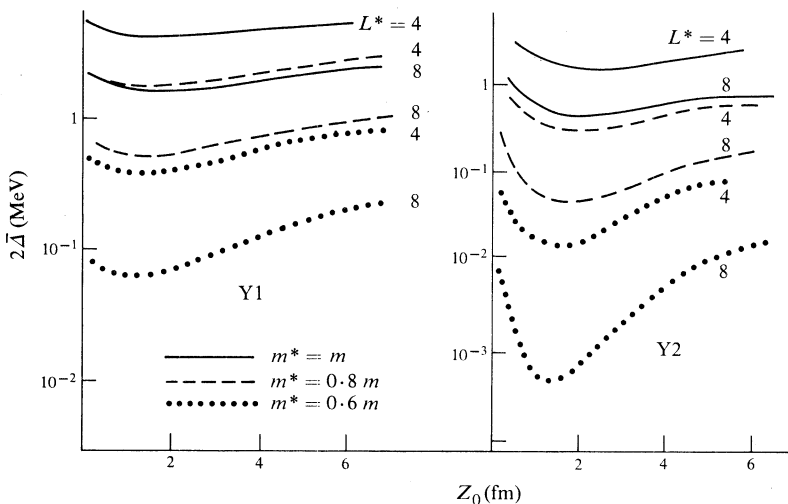


Fig. 5. Complete angle averaged Fourier components of the Y1 and Y3 potentials for  $Z_0 = 0$  and 3.25 fm and for four values of  $k$ . The effective length is 4 fm in both cases.

One purpose of this study was to gauge the effect of surface diffusivity upon the energy gap in nuclei, and to this end, the variation of the angle averaged energy gap as a function of  $Z_0$  for selected values of  $m^*$  and  $L^*$  for the potentials Y1 and Y2 are shown in Fig. 7. It is clear that, for moderately large values of the energy gap such as those that occur in nuclei, the dependence of the energy gap on the shape of the density profile ( $Z_0, L$ ) is much less than its dependence on the effective length  $L^*$  and that for still larger values of the energy gap it is almost independent of the shape of the density profile. However, specific effects of the surface region upon the effective mass have not been considered.



**Fig. 6.** Mass variation of the pairing energies for the Y1 and Y2 interactions compared with the mean (equation 31) of the data depicted by the dashed curves. The solid curves are the results found using a slope parameter  $Z_0 = 0$  and the dotted curve is for  $Z_0 = 3.25$  fm.



**Fig. 7.** Angle averaged energy gap  $2\bar{\Delta}$  for potentials Y1 and Y2 as a function of  $Z_0$  for selected values of the effective length and effective mass.

#### 4. Density Dependence of Effective Mass

In the foregoing it was shown that the energy gap was determined essentially by the ‘effective length’ of the slab model if the effective mass  $m^*$  was assumed independent of density. However, the ratio  $m^*/m$  which is about 0.6 in the nuclear interior is known to approach unity in the surface region (Bethe 1971). Hence, it is of interest to evaluate the single particle energies and effective mass from the definitions

$$\epsilon(\mathbf{k}) = \langle v | p^2/2m | v \rangle + \sum_{v'} \langle vv' | V | vv' - v'v \rangle, \tag{32}$$

$$\partial\epsilon(\mathbf{k})/\partial k |_{k=k_F} = \hbar^2 k_F/m^*(k_F), \tag{33}$$

where the wavefunctions  $\langle r | v \rangle$  are those of the slab model with a linear single particle potential, namely

$$\langle r | v \rangle = \psi(\mathbf{k}, r) \chi_{\frac{1}{2}m_s} \chi_{\frac{1}{2}m_t}, \quad (34)$$

and the interaction  $V$  is taken to be of the separable Yamaguchi type. For the purpose of evaluating the single particle energies only, the interaction is assumed to act in relative S states for both spin singlet and triplet configurations and the interaction chosen is that classified Y1 previously but extended to include a triplet state component, the parameter values of which are given in Table 1 under the entry Y1T. This combination was selected because of infinite nuclear matter results (Day 1967) and since the Y1 interaction best reproduced the average pairing energy data. The properties of the Airy functions then allow us to deduce that

$$\begin{aligned} \varepsilon(\mathbf{k}) = & \hbar^2 k^2 / 2m - (\hbar^2 / 3m) k_z^2 A^{-2}(k_z) (2Z_0 k_z^2 / k_F^2 - \sin 2\delta / 2k_z) \\ & + \frac{3}{4\pi^2} \int d\mathbf{k}' A^{-2}(k_z) \langle \mathbf{k}\mathbf{k}' | V | \mathbf{k}\mathbf{k}' \rangle, \end{aligned} \quad (35)$$

from which, by numerical differentiation, we ascertain the effective mass whose variation as a function of  $k_z$  for selected values of the parameters  $Z_0$  and  $L^*$  is given in Fig. 8. The effective mass is strongly anisotropic and for moderate values of the parameter  $Z_0$  varies approximately from the infinite matter value at  $k_z = 0$ , to  $m^* = m$  or greater at  $k_z = k_F$ .

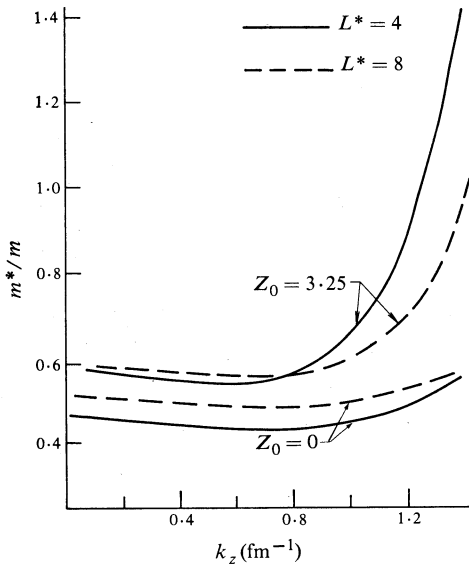


Fig. 8. Effective mass as a function of  $k_z$  for selected values of  $Z_0$  and effective length  $L^*$ .

The angle averaged effective mass is shown as a function of  $Z_0$  for selected values of  $L^*$  in Fig. 9, and in the case  $L^* = 4$  fm, although this quantity increases rapidly as a function of  $Z_0$ , its value at  $Z_0 = 3.25$  fm is about  $0.69m$ . This is somewhat smaller than the value  $m^* = 0.804m$  required to reproduce pairing energy data. However, the reduction of the effective mass below its infinite matter value for small  $Z_0$  results from the geometry of the slab model and hence would not occur in a

spherical nucleus. Therefore, it is expected that a more enhanced effective mass with surface thickness would be obtained in the latter case. Associated with the reduced effective mass for small  $Z_0$  is the collapse of the 'slab' nucleus, as is shown in Fig. 10 which displays the energy per particle as a function of  $L^*$  for selected values of  $Z_0$ .

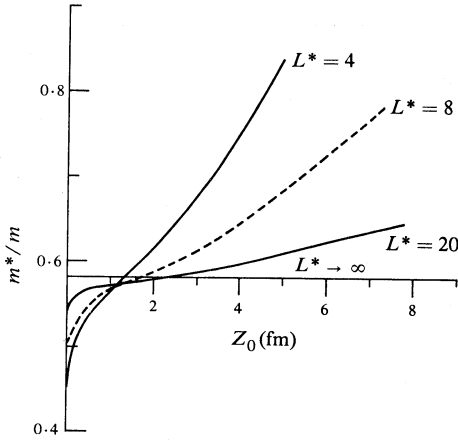


Fig. 9. Angle averaged effective mass as a function of  $Z_0$  for selected values of the effective length  $L^*$ .

Indeed, in order to make the nucleus stable in size ( $L^*$ ), it is necessary to restrict values of the surface thickness to 2 fm or greater. That the instability of the 'slab' nucleus is a result of its small surface contribution to the total energy can be seen from the following argument. Consider a slab and a sphere with equivalent density profiles such that the skin thickness (90%-10% density) and width of central region (90%-90% density) are  $\Delta R$  and  $2R$  respectively. Then the ratio of volume of surface region to that of the inner region is given by  $3\Delta R/R$  and  $\Delta R/R$  for the sphere and slab respectively.

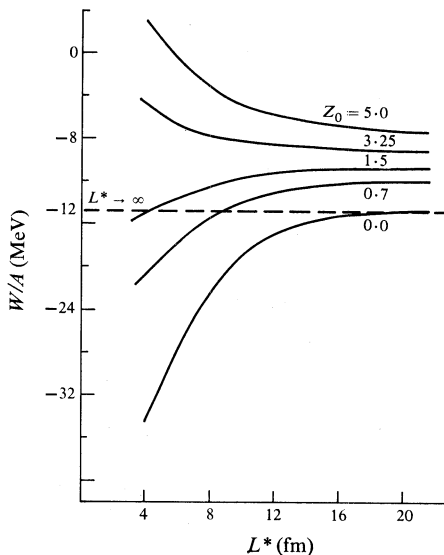
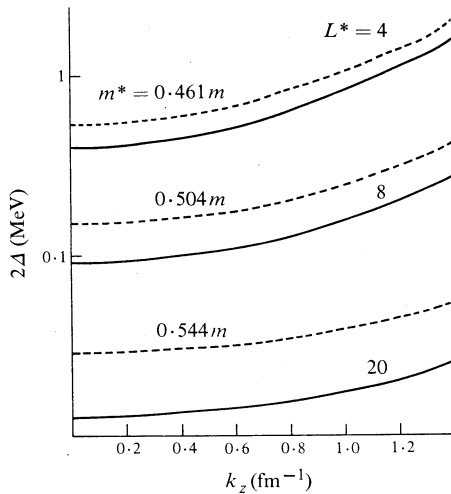


Fig. 10. Energy per particle as a function of effective length  $L^*$  of the slab of nuclear matter for various values of the slope parameter  $Z_0$ .

As the effective mass approximation causes the energy denominators in the gap equation to be in error outside the thin momentum shell about the Fermi surface, the energy gap has been recalculated using the single particle energies one obtains with the value  $Z_0 = 0$  and selected values of  $L^*$ . The results are given in Fig. 11, along with the estimate one finds by using  $\hbar^2(k^2 - k_F^2)/2\bar{m}^*$ , where  $\bar{m}^*$  is the angle averaged effective mass at the Fermi surface. The latter results are displayed by the dashed curves in the figure and are noticeably but not dramatically larger than the evaluated (solid curves) results.



**Fig. 11.** Comparison of the density variation of the energy gap in the slab model for various effective lengths with single particle energies obtained in the effective mass approximation (dashed curves) and evaluated as described in the text (solid curves). Here  $Z_0 = 0$ .

## 5. Conclusions

In the context of a slab model, the density dependence of the energy gap in nuclei has been studied for a number of separable interactions and a correlation has emerged between the strength of the repulsive core of the interaction and the behaviour of the energy gap in the model. For interactions with softer cores the energy gap increases strongly as the effective length  $L^*$  of the slab is reduced, while for the interaction studied with the largest repulsive core the energy gap decreased as  $L^*$  was reduced. From our considerations, it is clear that the unrealistic geometry of the slab model causes an underestimate of the attraction of the pairing matrix element for a hard core potential. Hence it remains to be seen whether such large differences in behaviour of the energy gap for such a potential would persist in more realistic models. The main feature to emerge from our calculations was the small dependence of the energy gap on the shape of the density profile compared with its dependence on  $L^*$ . Thus the energy gap is not essentially a surface phenomenon although the rate of vanishing of the nuclear wavefunctions at large distances may still affect the magnitude of the gap substantially.

Hence, in summary, the presence of the nuclear surface by enhancing the low momentum components of the pairing matrix elements leads to an enlarged energy gap in finite nuclei. However, this enhancement of the energy gap does not depend so much on the density profile as on the effective volume in which the nuclei are contained.

Finally, neither the use of the effective mass approximation nor direct evaluation (within the slab model) of the single particle energies were sufficient to account for the value of the effective mass required to fit pairing energy data. However, the results of the slab model for the soft core separable potential considered are in doubt since there is not proper saturation. A by-product of this behaviour is that for small values of the skin thickness the effective mass lies below its infinite matter limit and hence we are led to expect an enlarged value of the effective mass from realistic models. Such models would need to possess the correct geometry relevant to nuclear shapes and also a variable skin thickness.

### References

- Bethe, H. A. (1971). *Annu. Rev. Nucl. Sci.* **39**, 719.  
 Britt, H. C., Gibbs, W. B., and Griffin, J. J. (1965). *Phys. Rev.* **139**, 8354.  
 Day, B. D. (1967). *Rev. Mod. Phys.* **39**, 719.  
 Emery, V. J., and Sessler, A. M. (1960). *Phys. Rev.* **119**, 248.  
 Griffin, J. J. (1963). *Phys. Rev.* **132**, 2204.  
 Henley, E. M., and Wilets, L. (1963). *Phys. Rev.* **133**, B1118.  
 Ishihara, T., Tamogachi, R., Tanaka, H., and Yasuno, M. (1963). *Prog. Theor. Phys. Jpn* **30**, 601.  
 Jakeman, E., and Moszkowski, S. A. (1966). *Phys. Rev.* **141**, 933.  
 Kennedy, R. C. (1966a). *Nucl. Phys.* **89**, 623.  
 Kennedy, R. C. (1966b). *Phys. Rev.* **144**, 804.  
 Kennedy, R. C., Wilets, L., and Henley, E. M. (1964a). *Phys. Rev. Lett.* **12**, 36.  
 Kennedy, R. C., Wilets, L., and Henley, E. M. (1964b). *Phys. Rev.* **133**, 1131.  
 Kuvatov, K. C., Okolovitch, V. N., and Smirenkin, G. N. (1970). *ZhSTF (Fis. Red.)* **11**, 42.  
 Moretto, L. G., Gatti, R. C., Thompson, S. G., Huizenga, J. B., and Rasmussen, A. V. (1969). *Phys. Rev.* **178**, 1845.  
 Natowity, J. B., and Chulick, E. J. (1971). *Nucl. Phys. A* **172**, 185.  
 Nemirovsky, P. E., and Adamchuk, Yu. V. (1962). *Nucl. Phys.* **39**, 551.  
 Stepien, W., and Szymanski, Z. (1968). *Phys. Lett. B* **26**, 181.  
 Strobel, G. L. (1968). *Nucl. Phys. A* **116**, 465.  
 Thompson, C. J. (1965). *Phys. Lett.* **14**, 146.  
 Thompson, C. J., and Waghmare, Y. R. (1966). *Nucl. Phys.* **77**, 477.

### Appendix. Pairing Matrix Elements

The pairing matrix elements  $G(\mathbf{k}, \mathbf{k}')$  defined in equation (24) for the model described in the text for both the Yamaguchi and gaussian forms of the potential have the form

$$G(\mathbf{k}, \mathbf{k}') = \iiint d\mathbf{R} d\mathbf{r} d\mathbf{r}' V(\mathbf{r}, \mathbf{r}') \\ \times \psi^*(\mathbf{k}, \mathbf{R} + \frac{1}{2}\mathbf{r}) \psi^*(-\mathbf{k}, \mathbf{R} - \frac{1}{2}\mathbf{r}) \psi(\mathbf{k}', \mathbf{R} + \frac{1}{2}\mathbf{r}') \psi(-\mathbf{k}', \mathbf{R} - \frac{1}{2}\mathbf{r}'), \quad (\text{A1})$$

where the wavefunction  $\psi(\mathbf{k}, \mathbf{r})$  is specified in equations (2) and (4). For convenience, consider the potential in the form

$$V(\mathbf{r}, \mathbf{r}') = \lambda \omega(\mathbf{r}) \omega(\mathbf{r}'), \quad (\text{A2})$$

where the form factor  $\omega(\mathbf{r})$  is to be chosen appropriately for the Yamaguchi and gaussian interactions, and on substitution into equation (A1) one obtains

$$G(\mathbf{k}, \mathbf{k}') = \frac{32\lambda}{S} A^2(k_z) A^2(k'_z) \int_{-\frac{1}{2}L}^{\infty} dz |I(k_{\perp}, k_z, z)|^2, \quad (\text{A3})$$

where

$$I(k_{\perp}, k_z, z) = \int_0^{\infty} du \phi(k_z, z+u) \phi(k_z, z-u) h_{k_{\perp}}(u), \quad (\text{A4})$$

$$k_{\perp} = (k_x^2 + k_y^2)^{\frac{1}{2}}. \quad (\text{A5})$$

Defining

$$\beta_k = (\beta^2 + k_{\perp}^2)^{\frac{1}{2}}, \quad (\text{A6})$$

one has

$$h_{k_{\perp}}(u) = (2\pi/\beta_k) \exp(-2\beta_k u) \quad (\text{A7})$$

$$= (\pi/\alpha) \exp(-k_{\perp}^2/4\alpha - 4\alpha u^2) \quad (\text{A8})$$

for the Yamaguchi and gaussian interactions respectively.

In the case of the Yamaguchi interaction, we obtain for  $I(k_{\perp}, k_z, z)$  the explicit expression

$$I(k_{\perp}, k_z, z) = \sum_{i=0}^2 I_i(k_{\perp}, k_z, z), \quad (\text{A9})$$

where

$$I_0 = (\pi/2\beta_k^2) \{1 - \Theta(-z)\} \{\beta_k^2/(\beta_k^2 + k_z^2) - \cos(2k_z z + 2\delta)\}, \quad (\text{A10a})$$

$$I_1 = \{\pi \exp(2\beta_k z)/2(\beta_k^2 + k_z^2)\} \{1 - \Theta(-z)\} (a_k \cos 2k_z z - b_k \sin 2k_z z), \quad (\text{A10b})$$

with

$$a_k = (1 + k_z^2/\beta_k^2) \cos 2\delta - 1, \quad b_k = (1 + k_z^2/\beta_k^2) \sin 2\delta + k_z/\beta_k, \quad (\text{A11})$$

and

$$\begin{aligned} I_2 = & \{\sin \delta / \text{Ai}(-K)\} \int_{|z|}^{\infty} du h_{k_{\perp}}(u) \\ & \times \sin\{k_z(z-u) + \delta\} \text{Ai}\{(k_F^2/Z_0)^{1/3}(z+u) - K\} \\ & + \{\Theta(z) \sin^2 \delta / \text{Ai}^2(-K)\} \int_0^z du h_{k_{\perp}}(u) \\ & \times \text{Ai}\{(k_F^2/Z_0)^{1/3}(z+u) - K\} \text{Ai}\{(k_F^2/Z_0)^{1/3}(z-u) - K\}, \end{aligned} \quad (\text{A12})$$

in which terms of order  $h_{k_{\perp}}(L)$  have been neglected.

For the case of the gaussian the expression for  $I_2$  is the same but with the appropriate choice of  $h_{k_{\perp}}(u)$  the relevant expressions for  $I_0(k_{\perp}, k_z, z)$  and  $I_1(k_{\perp}, k_z, z)$  are

$$I_0 = \{1 - \Theta(-z)\} (\pi/4\alpha)^{3/2} \exp(-k_{\perp}^2/4\alpha) \{\exp(k_z^2/4\alpha) - \cos(2k_z z + 2\delta)\}, \quad (\text{A13})$$

$$\begin{aligned} I_1 = & \{1 - \Theta(-z)\} (\pi/4\alpha)^{3/2} \exp(-k_{\perp}^2/4\alpha - 4\alpha z^2) g(-2\alpha^{\frac{1}{2}}z) \left\{ \cos(2k_z z) - 1 \right\} / 4\alpha^{\frac{1}{2}}z \\ & + 2 \sum_{n=1}^{\infty} \left( \exp(-n^2/4) / (n^2 + 4\alpha z^2) \right) f_n(-2\alpha^{\frac{1}{2}}z, k_z/2\alpha^{\frac{1}{2}}), \end{aligned} \quad (\text{A14})$$

where

$$f_n(x, y) = 2x - 2x \cosh ny \cos 2xy + n \sinh ny \sin 2xy, \quad (\text{A15})$$

$$g(x) = 0.25483t - 0.2845t^2 + 1.4214t^3 - 1.4532t^4 + 1.0614t^5, \quad (\text{A16})$$

in which

$$t = (1 + 0.3276x)^{-1}. \quad (\text{A17})$$

In the case of the Yamaguchi interaction, evaluation of the pairing matrix elements is facilitated by using the expansion (ignoring terms involving  $\exp(-\beta L)$ )

$$\begin{aligned} G(\mathbf{k}, \mathbf{k}') &= (4\pi^2\lambda/S)A^2(k_z)A^2(k'_z) \\ &\times \left( L/\{(\beta_k^2 + k_z^2)/(\beta_{k'} + k'_z)\} + \pi(\beta_k \beta_{k'})^{-2}\delta(k_z - k'_z) \right. \\ &+ (\beta_k \beta_{k'})^{-2}\{\sin 2(\delta + \delta')/2(k_z + k'_z) + \sin 2(\delta - \delta')/2(k_z - k'_z)\} \\ &- 2 \sin 2\delta/\{2k_z \beta_k^2(\beta_{k'}^2 + k'^2_z)\} - 2 \sin 2\delta'/\{2k'_z \beta_{k'}^2(\beta_k^2 + k_z^2)\} \\ &+ F_1(k_z, \beta_k; k'_z, \beta_{k'}) + F_1(k'_z, \beta_{k'}; k_z, \beta_k) + F_2(k_z, \beta_k; k'_z, \beta_{k'}) \\ &+ F_2(k'_z, \beta_{k'}; k_z, \beta_k) + F_2(k_z, \beta_k; -k'_z, \beta_{k'}) \\ &+ F_2(k'_z, \beta_{k'}; -k_z, \beta_k) + F_3(k_z, \beta_k; k'_z, \beta_{k'}) \\ &+ F_3(k_z, \beta_k; -k'_z, \beta_{k'}) + 2 \int_{-\infty}^{\infty} dz I_2(k_{\perp}, k_z, z) I_2(k'_{\perp}, k'_z, z) \\ &+ 2 \int_{-\infty}^{\infty} dz I_2(k'_{\perp}, k'_z, z) \{I_0(k_{\perp}, k_z, z) + I_1(k_{\perp}, k_z, z)\} \\ &+ 2 \int_{-\infty}^{\infty} dz I_2(k_{\perp}, k_z, z) \{I_0(k'_{\perp}, k'_z, z) + I_1(k'_{\perp}, k'_z, z)\} \Big), \quad (\text{A18}) \end{aligned}$$

where

$$\begin{aligned} F_1(k_z, \beta_k; k'_z, \beta_{k'}) &= (a_k \beta_{k'} + b_k k'_z)(\beta_k^2 + k_z^2)^{-1}(\beta_{k'}^2 + k'^2_z)^{-2}, \\ F_2(k_z, \beta_k; k'_z, \beta_{k'}) &= [2\beta_k^2(\beta_{k'}^2 + k'^2_z)\{\beta_{k'}^2 + (k_z + k'_z)^2\}]^{-1} \\ &\times \beta_{k'}[\sin 2\delta \{b_{k'} - a_k(k_z + k'_z)/\beta_{k'}\} \\ &- \cos 2\delta \{a_{k'} + b_k(k_z + k'_z)/\beta_{k'}\}], \quad (\text{A19}) \end{aligned}$$

$$\begin{aligned} F_3(k_z, \beta_k; k'_z, \beta_{k'}) &= \{(\beta_k + \beta_{k'})(a_k a_{k'} + b_k b_{k'}) + (k_z - k'_z)(a_k b_k - b_{k'} a_{k'})\} \\ &\times [2(\beta_k^2 + k_z^2)(\beta_{k'}^2 + k'^2_z)\{(\beta_k + \beta_{k'})^2 + (k_z - k'_z)^2\}]^{-1}. \quad (\text{A20}) \end{aligned}$$

The remaining integrals must be found by numerical means.

Likewise evaluation of the pairing matrix elements associated with the gaussian interaction is facilitated by using the expanded expression

$$\begin{aligned}
G(\mathbf{k}, \mathbf{k}') &= (\pi^3/4S\alpha^3)A^2(k_z)A^2(k'_z)\exp\{-(k_\perp^2+k'_\perp^2)/4\alpha\} \\
&\times \left( L\exp\{-(k_z^2+k'_z{}^2)/4\alpha\} + \pi\delta(k_z-k'_z) \right. \\
&\quad - \exp(-k_z^2/4\alpha)\sin 2\delta' - \exp(-k'_z{}^2/4\alpha)\sin 2\delta \\
&\quad + \sin 2(\delta+\delta')/2(k_z+k'_z) + \sin 2(\delta-\delta')/2(k_z-k'_z) \\
&\quad + 2\int_{-\infty}^{\infty} dz I_0(k_\perp, k_z, z)\{I_1(k'_\perp, k'_z, z) + I_2(k'_\perp, k'_z, z)\} \\
&\quad + 2\int_{-\infty}^{\infty} dz I_0(k'_\perp, k'_z, z)\{I_1(k_\perp, k_z, z) + I_2(k_\perp, k_z, z)\} \\
&\quad \left. + 2\int_{-\infty}^{\infty} dz \{I_1(k_\perp, k_z, z) + I_2(k_\perp, k_z, z)\}\{I_1(k'_\perp, k'_z, z) + I_2(k'_\perp, k'_z, z)\} \right).
\end{aligned}
\tag{A21}$$

Manuscript received 6 November, accepted 23 December 1981